Pitchfork bifurcation and vibrational resonance in a fractional-order Duffing oscillator

J H YANG[1,*], M A F SANJUÁN[2], W XIANG[3] and H ZHU[1]

[1]School of Mechanical and Electrical Engineering, China University of Mining and Technology, Xuzhou 221116, People's Republic of China
[2]Nonlinear Dynamics, Chaos and Complex Systems Group, Departamento de Física, Universidad Rey Juan Carlos, Tulipán s/n, 28933 Móstoles, Madrid, Spain
[3]Department of Mathematics and Computer Science, Huainan Normal University, Huainan 232038, People's Republic of China
*Corresponding author. E-mail: jianhuayang@cumt.edu.cn

Abstract. The pitchfork bifurcation and vibrational resonance are studied in a fractional-order Duffing oscillator with delayed feedback and excited by two harmonic signals. Using an approximation method, the bifurcation behaviours and resonance patterns are predicted. Supercritical and subcritical pitchfork bifurcations can be induced by the fractional-order damping, the exciting high-frequency signal and the delayed time. The fractional-order damping mainly determines the pattern of the vibrational resonance. There is a bifurcation point of the fractional order which, in the case of double-well potential, transforms vibrational resonance pattern from a single resonance to a double resonance, while in the case of single-well potential, transforms vibrational resonance from no resonance to a single resonance. The delayed time influences the location of the vibrational resonance and the bifurcation point of the fractional order. Pitchfork bifurcation is the necessary condition for the double resonance. The theoretical predictions are in good agreement with the numerical simulations.

Keywords. Supercritical pitchfork bifurcation; subcritical pitchfork bifurcation; vibrational resonance; time delay feedback.

PACS Nos 05.45.−a; 02.30.Ks; 45.10.Hj

1. Introduction

Vibrational resonance (VR) is a phenomenon originally found by Landa and McClintock [1]. For the VR phenomenon to appear, a nonlinear system needs to be excited by two harmonic driving signals, a low- and a high-frequency signal. As a result, the response amplitude of the system to the low-frequency signal vs. the amplitude of the high-frequency

signal presents a resonance-like behaviour. In other words, the weak low-frequency signal can be amplified excellently by an appropriate high-frequency signal. Since biharmonical signals are applied in a wide range of disciplines, VR has been investigated in different kinds of systems by using theoretical, numerical and experimental methods [2–14]. Recently, the results of VR in fractional-order systems were reported by Yang and Zhu, and they found that the fractional-order damping is a key point to induce different resonance patterns [15,16]. Fractional-order systems have profound impact on many scientific and engineering fields such as rheology, viscoelasticity, electrochemistry, bioengineering, mechanics, automatic control and signal processing [17–20]. Hence, it is important to study the dynamics of different fractional-order systems. Here we consider the VR phenomenon in the fractional-order Duffing oscillator with time delay feedback. The equation of motion of the system we analyse here is given by

$$\frac{\mathrm{d}^\alpha x(t)}{\mathrm{d}t^\alpha} + \omega_0^2 x(t) + \beta x^3(t) + \gamma x(t - \tau) = f \cos(\omega t) + F \cos(\Omega t), \qquad (1)$$

where α is the order of the fractional-order damping and this term is very important for the VR pattern. There are several definitions commonly used for the fractional-order differential operator that appears in eq. (1), such as the Riemann–Liouville (RL) definition, the Caputo definition and the Grünwald–Letnikov (GL) definition [21]. For the fractional-order differential operator in eq. (1), these three definitions are equivalent. Here, we use the GL definition due to its convenience in the discretization of the fractional-order operator. The GL definition is given by

$$\left.\frac{\mathrm{d}^\alpha x(t)}{\mathrm{d}t^\alpha}\right|_{t=kh} = \lim_{h \to 0} \frac{1}{h^\alpha} \sum_{j=0}^{k} (-1)^j \binom{\alpha}{j} x(kh - jh), \qquad (2)$$

where the binominal coefficients are

$$\binom{\alpha}{0} = 1, \quad \binom{\alpha}{j} = \frac{\alpha(\alpha - 1) \cdots (\alpha - j + 1)}{j!}, \quad \text{for } j \geq 1. \qquad (3)$$

The value of α usually lies in the range of 0–2. The strength of the linear time delay feedback is γ and τ is the delayed time. In eq. (1), the parameters satisfy $\beta > 0$, $f \ll 1$ and $\omega \ll \Omega$. In the absence of the external biharmonic signals and the delayed time, the potential of the system is $V(x) = \frac{1}{2}(\omega_0^2 + \gamma)x^2 + \frac{1}{4}\beta x^4$, and it has a double-well form when $\omega_0^2 + \gamma < 0$ while it has a single-well form when $\omega_0^2 + \gamma \geq 0$. For the special case $\alpha = 1$, the system degenerates the general delayed system, and the VR phenomenon for this case was studied thoroughly by Jeevarathinam *et al* [8].

The phenomenon of VR has been analysed in delayed and fractional-order systems [8,15,16]. However, earlier works have been mostly focussed on the response amplitude of the system. The specific roles of different parameters on the bifurcation behaviours and the connection between the bifurcation and resonance patterns have not yet been thoroughly investigated. This is the main motivation of our paper. The paper is organized as follows: In §2, the supercritical pitchfork bifurcation and the subcritical pitchfork bifurcation induced by different factors are studied. In §3, according to the theoretical predictions, the conditions for different vibrational resonance patterns are derived. The roles of

fractional-order damping and time delay feedback on VR will be investigated. In order to check the validity of the analytical results, several examples are verified by numerical simulations. Finally, in §4, some conclusions are offered.

2. Bifurcation analysis

Since the frequencies of the external perturbations have the property that $\omega \ll \Omega$, the method of separation of slow and fast motions can be used to compute the response amplitude of the system [22]. Let $x = X + \Psi$, where X and Ψ are the corresponding slow and fast variables with periods $2\pi/\omega$ and $2\pi/\Omega$ respectively. Then the motion of the system of eq. (1) becomes

$$\frac{d^\alpha X}{dt^\alpha} + \frac{d^\alpha \Psi}{dt^\alpha} + \omega_0^2 X + \omega_0^2 \Psi + \beta X^3 + \beta \Psi^3 + 3\beta X^2 \Psi + 3\beta X \Psi^2$$
$$+ \gamma X_\tau + \gamma \Psi_\tau = f\cos(\omega t) + F\cos(\Omega t), \tag{4}$$

with $X_\tau = X(t - \tau)$ and $\Psi_\tau = \Psi(t - \tau)$. The approximated solution of $\Psi(t)$ is given in the equation

$$\frac{d^\alpha \Psi}{dt^\alpha} + \omega_0^2 \Psi + \gamma \Psi_\tau = F\cos(\Omega t). \tag{5}$$

Let

$$\Psi = \frac{F}{\mu}\cos(\Omega t + \theta). \tag{6}$$

Substituting eq. (6) into eq. (5), one gets

$$\mu^2 = \left[\gamma\cos(\tau\Omega) + \Omega^\alpha\cos\left(\frac{\alpha\pi}{2}\right) + \omega_0^2\right]^2 + \left[\gamma\sin(\tau\Omega) - \Omega^\alpha\sin\left(\frac{\alpha\pi}{2}\right)\right]^2 \tag{7}$$

and

$$\theta = \tan^{-1}\frac{\gamma\sin(\tau\Omega) - \Omega^\alpha\sin(\alpha\pi/2)}{\Omega^\alpha\cos(\alpha\pi/2) + \omega_0^2 + \gamma\cos(\tau\Omega)}. \tag{8}$$

Then, substituting the solution of $\Psi(t)$ in eq. (4) and averaging the equation over the range $[0, 2\pi/\Omega]$, the equation for the slow motion is obtained as

$$\frac{d^\alpha X}{dt^\alpha} + C_1 X + \beta X^3 + \gamma X_\tau = f\cos(\omega t), \tag{9}$$

where

$$C_1 = \omega_0^2 + \frac{3\beta F^2}{2\mu^2}. $$

When $f = 0$ and $\tau = 0$, the effective potential function

$$V_{\text{eff}} = \frac{C_1 + \gamma}{2} x^2 + \frac{\beta}{4} x^4.$$

For this case, the equilibrium points for eq. (9) are given by

$$X_0^* = 0, \; X_\pm^* = \pm\sqrt{-\frac{C_1 + \gamma}{\beta}}. \tag{10}$$

When

$$F < F_c = \left[-\frac{2\mu^2(\omega_0^2 + \gamma)}{3\beta} \right]^{1/2}, \tag{11}$$

then $[(C_1 + \gamma)/\beta] < 0$ so that there are two stable equilibrium states $X_\pm^*$ and one unstable equilibrium state X_0^*. However, when

$$F \geq F_c = \left[-\frac{2\mu^2(\omega_0^2 + \gamma)}{3\beta} \right]^{1/2}, \tag{12}$$

then $[(C_1 + \gamma)/\beta] \geq 0$ so that there is only one stable state X_0^*. F_c is the bifurcation point which influences the stable states of the system in eq. (9).

If eq. (1) is a monostable oscillator, there is only one equilibrium point $X^* = 0$, and there is no bifurcation for this case. However, if eq. (1) is bistable, the stable states in eq. (10) depend on some other parameters. The pitchfork bifurcation occurs with the change of these parameters. When the stable equilibrium point turns from trivial to non-trivial, the supercritical pitchfork bifurcation occurs. On the contrary, when the stable equilibrium point turns from non-trivial to trivial, the subcritical pitchfork bifurcation occurs. When F is the control parameter, F_c is a critical point for the pitchfork bifurcation. The analytical result of F_c is given in eqs (11) and (12). However, when Ω, α or τ is treated as a control parameter, the analytical expression of the pitchfork bifurcation point Ω_c, α_c or τ_c which changes the stable equilibrium points of eq. (9) is difficult to obtain. For the double-well case, the bistable and monostable domains of eq. (9) are given on the F–α plane in figure 1a. From the boundary of the domains, we can see that the bifurcation point α_c increases with the increase of the parameter F. In figures 1b–1d, the subcritical pitchfork bifurcation induced by the parameter F is clearly shown for different values of the fractional order α. In figures 1e and 1f, the supercritical pitchfork bifurcation induced by the fractional order α is revealed for different values of F.

In figure 2a, the bistable domain and monostbale domain of eq. (9) are shown in the Ω–α plane. It is different from the information in figure 1a. Specifically, the value of the bifurcation point α_c decreases with the increase of the high-frequency Ω. In figures 2b–2d, for different values of the fractional order, the supercritical pitchfork bifurcation induced by the high-frequency Ω is shown. When the delayed time τ is a control parameter, the
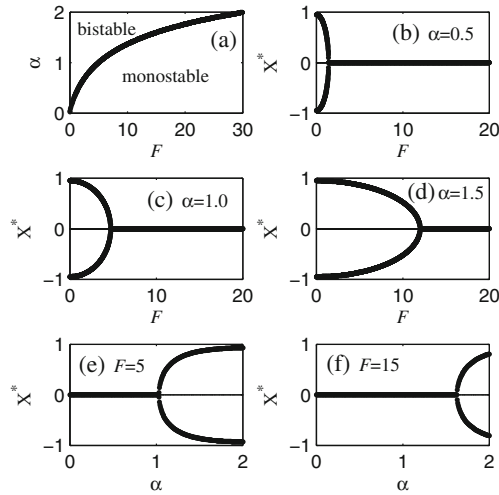
Figure 1. (**a**) Bistable and monostable regions in the F–α plane. (**b**)–(**d**) The subcritical pitchfork bifurcation induced by the parameter F. (**e**)–(**f**) The supercritical pitchfork bifurcation induced by the parameter α. The thick lines are stable states while the thin lines are unstable states. Other parameters are $\Omega = 6$, $\omega_0^2 = -1$, $\beta = 1$, $\gamma = 0.1$ and $\tau = 0.5$.

pitchfork bifurcation induced by the parameter τ is given in figure 3. With the increase of τ, the supercritical and subcritical pitchfork bifurcations occur periodically. This can also be obtained from eq. (10) because the parameter C_1 included in eq. (10) contains the
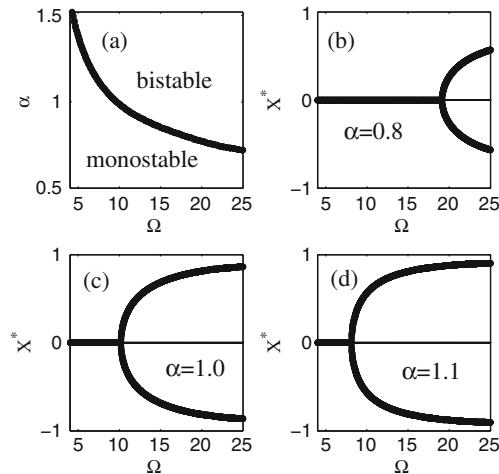
Figure 2. (**a**) Bistable and monostable regions in the Ω–α plane. (**b**)–(**d**) The supercritical pitchfork bifurcation induced by the parameter Ω. The thick lines are stable states while the thin lines are unstable states. Other parameters are $F = 8$, $\omega_0^2 = -1$, $\beta = 1$, $\gamma = 0.1$ and $\tau = 0.5$.
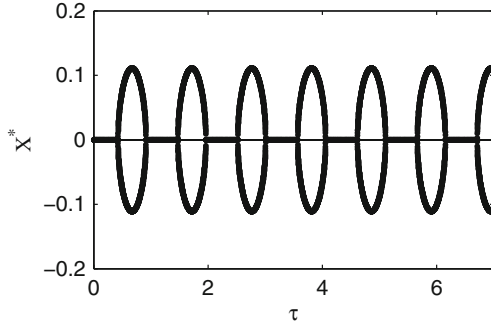
Figure 3. The supercritical and subcritical pitchfork bifurcations induced by the delayed time τ. The thick lines are stable states while the thin lines are unstable states. Other parameters are $F = 10$, $\Omega = 6$, $\omega_0^2 = -1$, $\beta = 1$, $\gamma = 0.1$ and $\alpha = 1.4$.

delayed time τ. Hence, the equilibrium point changes periodically with the delayed time τ with period $2\pi/\Omega$.

3. Resonance analysis

We consider the deviation Y from the stable equilibrium states X^*. Substituting $Y = X - X^*$ in eq. (9), we get the equation for Y:

$$\frac{d^\alpha Y}{dt^\alpha} + \omega_r^2 Y + 3\beta X^* Y^2 + \beta Y^3 + \gamma Y_\tau = f \cos(\omega t), \tag{13}$$

where $\omega_r^2 = C_1 + 3\beta X^{*2}$. Since $f \ll 1$, we ignore the nonlinear terms to seek the solution of Y in the equation

$$\frac{d^\alpha Y}{dt^\alpha} + \omega_r^2 Y + \gamma Y_\tau = f \cos(\omega t). \tag{14}$$

Letting $Y = A_L \cos(\omega t + \phi)$, and then substituting it in eq. (14), we obtain

$$A_L = \frac{f}{\sqrt{S}},$$
$$S = \left[\omega_r^2 + \gamma \cos(\omega\tau) + \omega^\alpha \cos\left(\frac{\alpha\pi}{2}\right)\right]^2 + \left[\gamma \sin(\omega\tau) - \omega^\alpha \sin\left(\frac{\alpha\pi}{2}\right)\right]^2, \tag{15}$$

and finally

$$\phi = \tan^{-1} \frac{\gamma \sin(\omega\tau) - \omega^\alpha \sin(\alpha\pi/2)}{\omega_r^2 + \gamma \cos(\omega\tau) + \omega^\alpha \cos(\alpha\pi/2)}. \tag{16}$$

The response amplitude of the output is defined as

$$Q = \frac{A_L}{f} = \frac{1}{\sqrt{S}}.$$

When S arrives at the local minimal, then VR occurs.

3.1 *The double-well potential case*

If we choose the parameter F as a control parameter, then VR occurs at the location $F = F_{VR}$ where F_{VR} is a root of the equation $(dS/dF) = 0$. When the equation $(dS/dF) = 0$ has no real root, then VR occurs at the location $F = F_c$. According to this viewpoint, for the double-well case $(\omega_0^2 + \gamma < 0)$, we get the following conclusions:

(a) If

$$\omega^\alpha \cos\left(\frac{\alpha\pi}{2}\right) \leq 2\omega_0^2 + 3\gamma - \gamma \cos(\omega\tau), \tag{17}$$

then, there is only one F_{VR}, i.e.,

$$F_{VR}^{(2)} = \left\{-\frac{2\mu^2}{3\beta}\left[\omega_0^2 + \omega^\alpha \cos\left(\frac{\alpha\pi}{2}\right) + \gamma \cos(\omega\tau)\right]\right\}^{1/2} > F_c. \tag{18}$$

The peak value of Q is

$$Q_{\max} = \frac{1}{|\gamma \sin(\omega\tau) - \omega^\alpha \sin(\alpha\pi/2)|}. \tag{19}$$

(b) If

$$2\omega_0^2 + 3\gamma - \gamma \cos(\omega\tau) < \omega^\alpha \cos\left(\frac{\alpha\pi}{2}\right) < \gamma - \gamma \cos(\omega\tau), \tag{20}$$

then there are two different F_{VR}, i.e., $F_{VR}^{(2)}$ in eq. (18) and

$$F_{VR}^{(1)} = \left\{\frac{\mu^2}{3\beta}\left[-2\omega_0^2 - 3\gamma + \omega^\alpha \cos\left(\frac{\alpha\pi}{2}\right) + \gamma \cos(\omega\tau)\right]\right\}^{1/2} < F_c. \tag{21}$$

At the points $F_{VR}^{(1)}$ and $F_{VR}^{(2)}$, the response amplitude has two identical local maxima that are expressed in eq. (19).

(c) If

$$\omega^\alpha \cos\left(\frac{\alpha\pi}{2}\right) \geq \gamma - \gamma \cos(\omega\tau), \tag{22}$$

one gets $F_{VR} = F_c$. The maximum of the response amplitude Q is
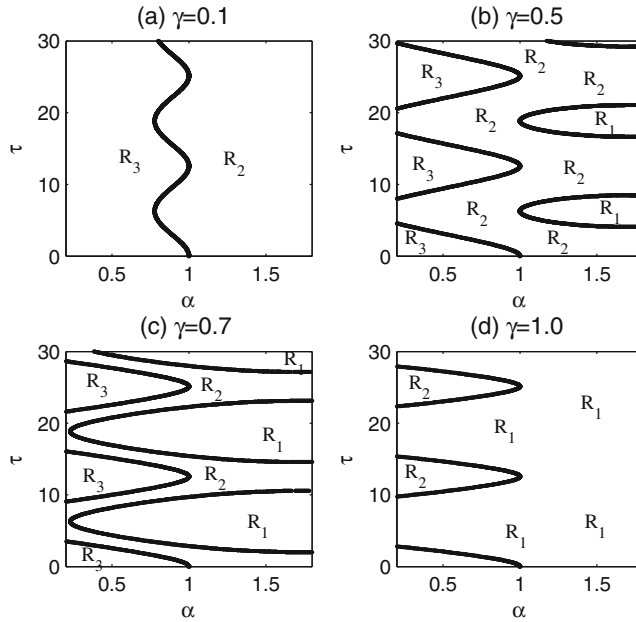
Figure 4. The regions correspond to different resonance patterns in the α–τ plane for the double-well case. R_1: the single resonance occurs at $F_{\text{VR}}^{(2)}$; R_2: the double resonance occurs at $F_{\text{VR}}^{(1)}$ and $F_{\text{VR}}^{(2)}$; R_3: the single resonance occurs at F_c. Other parameters are $\omega = 0.5$ and $\omega_0^2 = -1$.

$$Q_{\max} = \frac{1}{\sqrt{[\omega^\alpha \cos(\alpha\pi/2) - \gamma + \gamma \cos(\omega\tau)]^2 + [\gamma \sin(\omega\tau) - \omega^\alpha \sin(\alpha\pi/2)]^2}}.$$

(23)

According to these analytical predictions, the regions corresponding to different resonance patterns in the α–τ plane for the double-well case are shown in figure 4. The resonance patterns are influenced by the delayed time τ, the fractional order α and the delayed feedback strength γ. In region R_1, the single resonance occurs at $F_{\text{VR}}^{(2)}$; in region R_2, the double resonance occurs at $F_{\text{VR}}^{(1)}$ and $F_{\text{VR}}^{(2)}$; in region R_3, the single resonance occurs at F_c.

When the amplitude of the high-frequency signal is a control parameter, F_{VR} or F_c gives the location of the resonance, whose corresponding expressions are given above. In figure 5, with the change of the values of the delayed time τ, the conditions in eq. (20) or in eq. (22) can be satisfied. It results in F_c, $F_{\text{VR}}^{(1)}$ and $F_{\text{VR}}^{(2)}$ appearing periodically. Hence, the single resonance and the double resonance also occur periodically. The delayed time τ induces a bifurcation periodically in the number of the steady states at intervals of half period of the low-frequency signal. With the increase of the delayed time τ, F_{VR} varies periodically with two periods, which corresponds to the periods of the two exciting signals.

In figures 6a–6c, the bifurcation of F_{VR} induced by the fractional order α is clearly shown. In these subplots, α_c is the bifurcation point. VR is in the single-resonance pattern
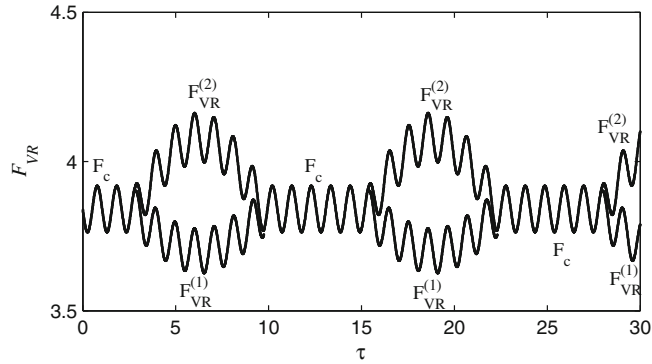
Figure 5. With the increase of the delayed time τ, F_c, $F_{VR}^{(1)}$ and $F_{VR}^{(2)}$ appear periodically for $\omega = 0.5$, $\Omega = 6.0$, $\beta = 1$, $\gamma = 0.1$, $\omega_0^2 = -1.0$ and $\alpha = 0.9$.

when α is located on the left side of α_c; while it is in the double-resonance pattern when α is located on the right side of α_c. Another fact is that α_c is influenced by the delayed time τ. In order to find out the effect of the delayed time τ on the location of the bifurcation point α_c, we give figure 6d in which α_c is clearly shown in the α–τ plane. With the increase of τ, the bifurcation point α_c varies periodically with the period of the low-frequency signal. Hence, the delayed time τ determines the location of the bifurcation point α_c. For a fixed value of the delayed time τ, there is only one bifurcation point α_c. However, there may be countless delay parameter values that satisfy one bifurcation point α_c. Also in figure 6d, we see that the bifurcation point α_c is always located on the left
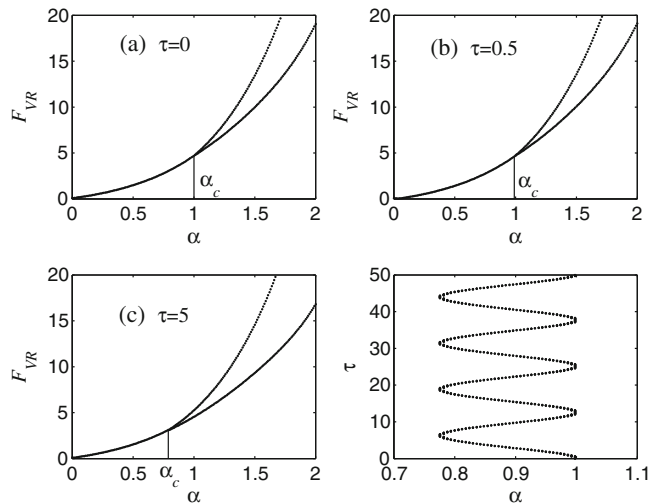
Figure 6. (**a**)–(**c**) The bifurcation of F_{VR} induced by the fractional order α for different delayed times. (**d**) The bifurcation point α_c on the α–τ plane. Other parameters are $\omega = 0.5$, $\Omega = 6.0$, $\omega_0^2 = -1.0$, $\beta = 1$ and $\gamma = 0.1$.

side of $\alpha = 1$. It can be obtained from eq. (22) in which the bifurcation point α_c should satisfy $\omega^\alpha \cos(\alpha\pi/2) = \gamma - \gamma \cos(\omega\tau)$. When γ is a small positive parameter, one has $\alpha_c \leq 1$. This equation is also the reason for the periodic variation of the bifurcation point α_c induced by the delayed time τ.

3.2 *The single-well potential case*

For the single-well case, $\omega_0^2 + \gamma \geq 0$, one has the following results:

(a) If

$$\omega^\alpha \cos\left(\frac{\alpha\pi}{2}\right) < -[\omega_0^2 + \gamma \cos(\omega\tau)], \tag{24}$$

then,

$$F_{\text{VR}} = \left\{-\frac{2\mu^2}{3\beta}\left[\omega_0^2 + \omega^\alpha \cos\left(\frac{\alpha\pi}{2}\right) + \gamma \cos(\omega\tau)\right]\right\}^{1/2}. \tag{25}$$

The maximum of the response amplitude Q is expressed by eq. (19).

(b) If

$$\omega^\alpha \cos\left(\frac{\alpha\pi}{2}\right) \geq -[\omega_0^2 + \gamma \cos(\omega\tau)], \tag{26}$$

then Q decreases with the increase of F. At $F = 0$, the response amplitude Q arrives at the local maximum

$$Q_{\max} = \frac{1}{\sqrt{[\omega^\alpha \cos(\alpha\pi/2) + \omega_0^2 + \gamma \cos(\omega\tau)]^2 + [\gamma \sin(\omega\tau) - \omega^\alpha \sin(\alpha\pi/2)]^2}}. \tag{27}$$

According to the conditions in eqs (24) and (26), the regions for single resonance and no-resonance pattern for the single-well case are given in figure 7. The line in each subplot denotes the equation $\omega^\alpha \cos(\alpha\pi/2) = -[\omega_0^2 + \gamma \cos(\omega\tau)]$. On the left side of the line, eq. (26) is satisfied, resulting in the no-resonance pattern for any value of F, while on the right side of the line, eq. (24) is satisfied, leading to the single-resonance pattern at F_{VR}.

Single resonance occurs for the single-well potential case when $F_{\text{VR}} > 0$. Figure 8 indicates that single resonance occurs only for some appropriate delayed time τ. For this case, $F_{\text{VR}} = 0$ and $F_{\text{VR}} > 0$ exist periodically. Hence, the no-resonance and single-resonance patterns of VR occur periodically as well. It can also be obtained from the condition in eq. (24) which means that single resonance occurs only when $\alpha > 1$. From figure 8, we know that the fractional-order damping has an important effect on the resonance pattern, and the delayed time τ influences the amplitude of F_{VR}, i.e., the location of the resonance.

In figure 9, the bifurcation of F_{VR} induced by the fractional-order damping is given. In figures 9a–9c, F_{VR} turns to $F_{\text{VR}} > 0$ from $F_{\text{VR}} = 0$ as α increases. It implies that VR turns to single-resonance pattern from a no-resonance pattern. The location of the bifurcation point α_c depends on the delayed time τ. In figure 9d, the bifurcation point α_c is given in the α–τ plane. α_c varies periodically with period $2\pi/\omega$ as τ increases.
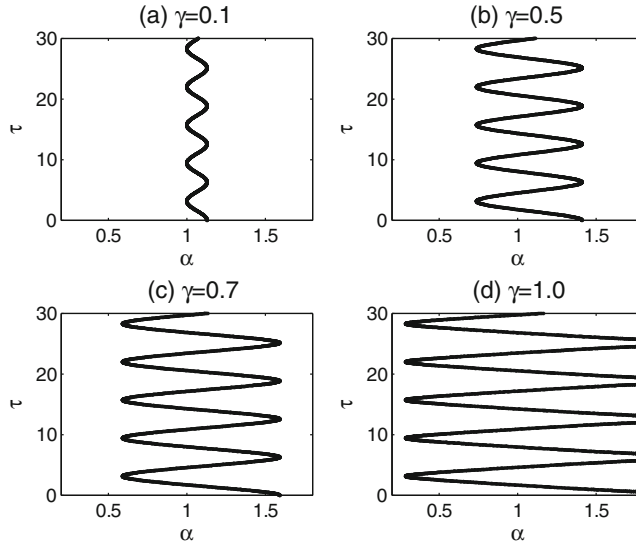
Figure 7. The regions correspond to different resonance patterns for the single-well case. In the α–τ plane, no resonance occurs on the left side of the line while single resonance occurs at F_{VR} on the right side of the line. Other parameters are $\omega = 1.0$, $\beta = 1.0$ and $\omega_0^2 = 0.1$.

Another fact is that α_c is always located on the right side of $\alpha = 1$. It is different from the double-well potential case in figure 6d. This is because single resonance occurs only when eq. (24) is satisfied resulting in the bifurcation point being located on the right side of $\alpha = 1$.

3.3 *Numerical simulations*

It is important to analyse the validity of the theoretical method used on VR in this paper. In this subsection, several examples will be given to verify the analytical predictions.
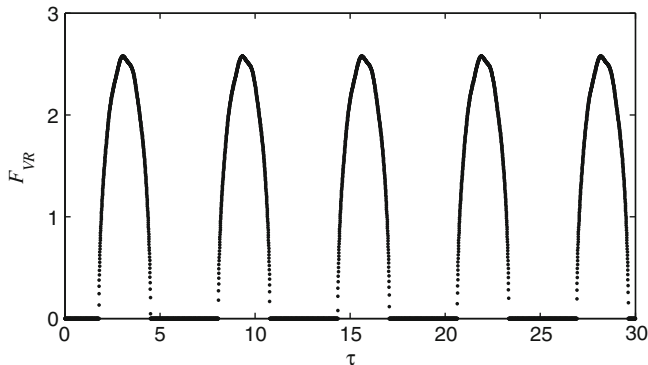
Figure 8. With the increase of the delayed time τ, $F_{\text{VR}} = 0$ and $F_{\text{VR}} > 0$ appear periodically for $\omega = 1$, $\Omega = 10$, $\beta = 1$, $\gamma = 0.1$, $\omega_0^2 = 0.1$ and $\alpha = 1.05$.
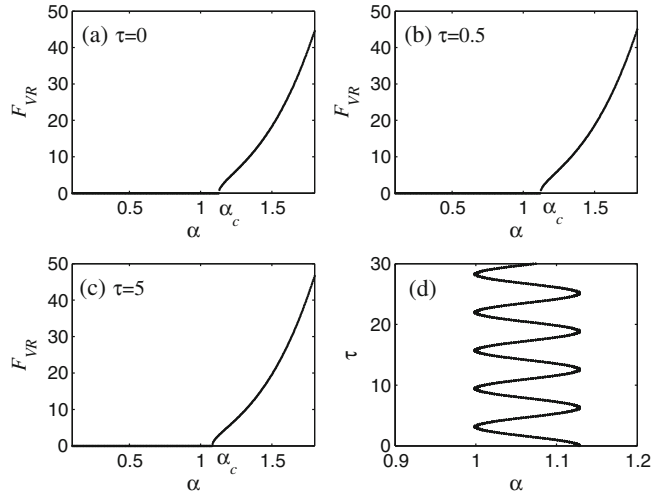
Figure 9. (a)–(c) The bifurcation of F_{VR} induced by the fractional order α for differ-ent delayed times. (d) The bifurcation point α_c on the α–τ plane. Other parameters are $\omega = 1$, $\Omega = 10$, $\beta = 1$, $\gamma = 0.1$ and $\omega_0^2 = 0.1$.

For the numerical simulations, the response amplitude is calculated by using the expression

$$Q = \frac{\sqrt{Q_{\sin}^2 + Q_{\cos}^2}}{f}, \tag{28}$$

with

$$Q_{\sin} = \frac{2}{rT} \int_0^{rT} x(t) \sin(\omega t) dt, \quad Q_{\cos} = \frac{2}{rT} \int_0^{rT} x(t) \cos(\omega t) dt,$$

where $T = 2\pi/\omega$ and r is a positive integer which should be chosen big enough. For convenience, we choose $r = 100$ in our simulations. According to refs [15,21], the Euler version of the integration of eq. (1) is given by

$$\begin{aligned} x_{k+1} = & -\sum_{j=1}^{k} w_j^\alpha x_{k+1-j} \\ & + \Delta t^\alpha \left[-\omega_0^2 x_k - \beta x_k^3 - \gamma x_{k-N} + f \cos(\omega k \Delta t) + F \cos(\Omega k \Delta t) \right], \end{aligned} \tag{29}$$

where $w_0^{(\alpha)} = 1$, $w_j^{(\alpha)} = (1 - \frac{\alpha+1}{j}) w_{j-1}^{(\alpha)}$, $j = 1, 2, 3, 4, \ldots, k$. Δt is the integral time step and $N = \tau/\Delta t$ is the number of discrete delayed time steps.

For the double-well case, the bifurcation of the resonance peak induced by the value of the fractional order α is given in figure 10. With the increase of α, the plot of Q turns to double resonance from single resonance in the three-dimensional theoretical curve
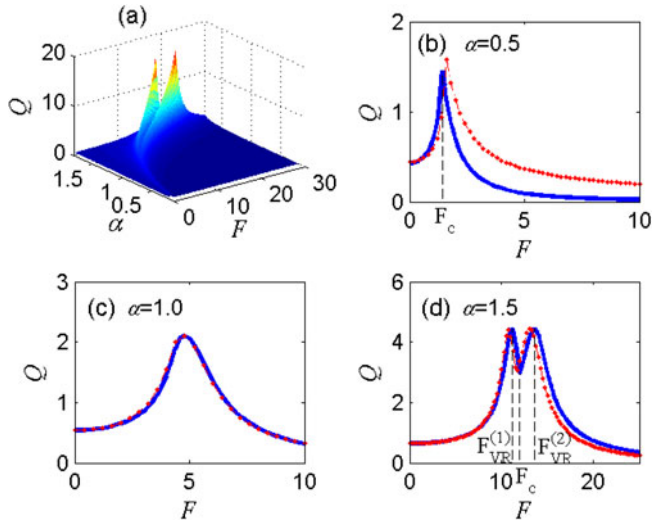
Figure 10. Different resonance patterns induced by the fractional order α for $\omega = 0.5$, $f = 0.025$, $\Omega = 6.0$, $\omega_0^2 = -1.0$, $\beta = 1$, $\gamma = 0.1$ and $\tau = 0.5$. (**a**) The three-dimensional theoretical curve of the response amplitude. (**b**) The single resonance occurs for $\alpha = 0.5$. (**c**) The resonance occurs when α is close to the bifurcation point α_c. (**d**) The double resonance occurs for $\alpha = 1.5$. The solid lines are the analytical results while the dotted lines are the numerical results.

as shown in figure 10a. When the condition in eq. (22) is satisfied, e.g., $\alpha = 0.5$ in figure 10b, Q arrives at the local maximum at $F = F_c$. In figure 10c, $\alpha = 1.0$, although eq. (20) is satisfied, α is very close to the bifurcation point α_c that is shown in figure 6b. It leads to double resonance which is hardly seen. When $\alpha = 1.5$, the condition in eq. (20) is satisfied, and it induces double resonance, as shown in figure 10d. For the double-resonance pattern, the response amplitude Q arrives at two identical peaks at the locations $F_{VR}^{(1)}$ and $F_{VR}^{(2)}$, while Q reaches a local minimum at $F = F_c$. Figure 10 proves the role of the fractional-order damping on the resonance pattern again.

For the single-well case, figure 11 shows that single resonance can be induced by the fractional-order damping. In figure 11a, the three-dimensional theoretical curve of the response amplitude Q vs. the values of α and F is given. A single resonance appears in the Q–F plot for increasing values of α. However, in the ordinary overdamped Duffing oscillator with a single-well potential, there is no resonance at all, and this fact can be easily derived from eq. (26). Figures 11b–11d give three specific examples for the information of Q in the two-dimensional curves. For $\alpha = 0.5$ and 1.0, eq. (26) is satisfied, and therefore Q arrives at the local maximum at $F = 0$. For these two situations, Q is a decreasing function of the variable F. When $\alpha = 1.5$, the condition in eq. (24) is satisfied, and hence resonance occurs at F_{VR} that is expressed in eq. (25), and the local maximum of Q is expressed by eq. (19). Figure 11 explains that the fractional-order damping changes the resonance pattern in the monostable Duffing oscillator once again. By comparing the theoretical predictions and numerical simulations in figures 10 and 11, we see that the errors between the analytical results and the numerical ones are very
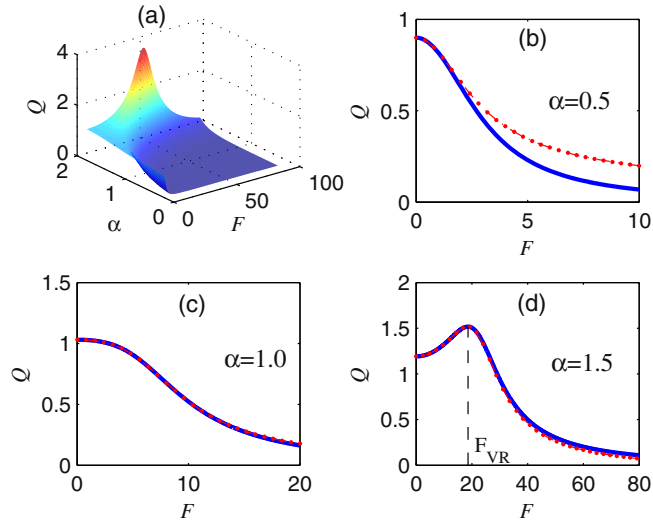
Figure 11. Different resonance patterns induced by the fractional order α for $\omega = 1$, $f = 0.025$, $\Omega = 1.0$, $\omega_0^2 = 0.1$, $\beta = 1$, $\gamma = 0.1$ and $\tau = 0.5$. (**a**) The three-dimensional theoretical curve of the response amplitude. (**b**) and (**c**) There is no resonance for $\alpha = 0.5$ or $\alpha = 1.0$. (**d**) The single resonance occurs for $\alpha = 1.5$. The solid lines are the analytical results while the dotted lines are the numerical results.

small. The analytical results of Q are in good agreement with the numerical ones, which confirms our theoretical analysis.

4. Conclusions

In the present paper, the pitchfork bifurcation and vibrational resonance in a delayed fractional-order Duffing oscillator are investigated for double-well potential and the single-well potential respectively. Based on the vibrational mechanism, the method of separation of slow and fast motions is used to predict the bifurcation and resonance. We find that the amplitude of the high-frequency signal induces the subcritical pitch-fork bifurcation, while the frequency of the high-frequency signal and the value of the fractional-order induces supercritical pitchfork bifurcation. The delayed time induces both subcritical and supercritical pitchfork bifurcations. We also find that not only the delayed time but also the value of the fractional-order induce different resonance patterns. The effects of the fractional damping and the time delay feedback on the VR phenomenon are very different. The value of the fractional order mainly determines the pattern of VR. With the change of the fractional order, the VR pattern transforms itself between single resonance and double resonance for the double-well potential case, and between no resonance and single resonance for the single-well potential case. There is a bifurcation point of the fractional order to distinguish these different resonance patterns. The delayed parameter affects the location and the peak value of VR, and it also affects the location of

the bifurcation point of the fractional order. The connection between bifurcation and resonance is that the pitchfork bifurcation is the necessary condition for the double-resonance pattern. In order to confirm the validity of the theoretical analysis, some numerical computed examples are given. The theoretical predictions and the numerical simulations are in good agreement. The results in this paper contribute to a better understanding of the VR phenomenon in the fractional and delayed systems.

Acknowledgements

References

[1] P S Landa and P V E McClintock, *J. Phys. A* **33**, L433 (2000)
[2] I I Blekhman and P S Landa, *Int. J. Non-Linear Mech.* **39**, 421 (2004)
[3] S Jeyakumari, V Chinnathambi, S Rajasekar and M A F Sanjuán, *Phys. Rev. E* **80**, 046608 (2009)
[4] C Yao and M Zhan, *Phys. Rev. E* **81**, 061129 (2010)
[5] J Casado-Pascual and J P Baltanás, *Phys. Rev. E* **69**, 046108 (2004)
[6] V N Chizhevsky and G Giacomelli, *Phys. Rev. E* **77**, 051126 (2008)
[7] J H Yang and X B Liu, *J. Phys. A* **43**, 122001 (2010)
[8] C Jeevarathinam, S Rajasekar and M A F Sanjuán, *Phys. Rev. E* **83**, 066205 (2011)
[9] B Deng, J Wang and X Wei, *Chaos* **19**, 013117 (2009)
[10] V N Chizhevsky, E Smeu and G Giacomelli, *Phys. Rev. Lett.* **91**, 220602 (2003)
[11] J P Baltanás, L López, I I Blechman, P S Landa, A Zaikin, J Kurths and M A F Sanjuán, *Phys. Rev. E* **67**, 066119 (2003)
[12] E Ullner, A Zaikin, J García-Ojalvo, R Bascones and J Kurths, *Phys. Lett. A* **312**, 348 (2003)
[13] V N Chizhevsky, *Int. J. Bifurcat. Chaos* **18**, 1767 (2008)
[14] A Ichiki, Y Tadokoro and M Takanashi, *J. Phys. A* **45**, 385101 (2012)
[15] J H Yang and H Zhu, *Chaos* **22**, 013112 (2012)
[16] J H Yang and H Zhu, *Commun. Nonlinear Sci. Numer. Simulat.* **18**, 1316 (2013)
[17] L Debnath, *Int. J. Math. Math. Sci.* **54**, 3413 (2003)
[18] J Sabatier, O P Agrawal and J A Tenreiro Machado, *Advances in fractional calculus: Theoretical developments and applications in physics and engineering* (Springer, Berlin, 2007)
[19] R Magin, *Comput. Math. Appl.* **59**, 1586 (2010)
[20] J T Machado, V Kiryakova and F Mainardi, *Commun. Nonlinear Sci. Numer. Simulat.* **16**, 1140 (2011)
[21] C A Monje, Y Chen, B M Vinagre, D Xue and V Feliu, *Fractional-order systems and controls* (Springer, London, 2010)
[22] I I Blekhman, *Vibrational mechanics* (World Scientific, Singapore, 2000)